Energy Materials

Article

Electronic modification of NaCrO$_2$ *via* Ni^{2+} substitution as efficient cathode for sodium-ion batteries

Jingyao Cai[1], Yanbing Zhu[1], Zhiguo Zhang[1], Jiandong Zhang[1], Liyuan Tian[2], Pengkun Gao[3], Yali Zhang[3], Mingkui Wang[1,2], Yan Shen[1,*]

[1]Wuhan National Laboratory for Optoelectronics, Huazhong University of Science and Technology, Wuhan 430074, Hubei, China.
[2]China-EU Institute for Clean and Renewable Energy, Huazhong University of Science and Technology, Wuhan 430074, Hubei, China.
[3]PYTES (Shandong) Energy Technology Co. Ltd., Building 1, High-Tech Industrial Park, Weishan County, Jining 272000, Shandong, China.

***Correspondence to:** Prof. Yan Shen, Wuhan National Laboratory for Optoelectronics, Huazhong University of Science and Technology, Luoyu Road 1037, Wuhan 430074, Hubei, China. E-mail: ciac_sheny@mail.hust.edu.cn

Abstract

The feature of high theoretical capacity, long thermal stability, and low-cost fabrication offers the layered transition metal oxide NaCrO$_2$ as an excellent candidate for sodium-ion batteries. Here, we show an effective method for electronic modulation of NaCrO$_2$ by partial substitution of Cr^{3+} with low-valent Ni^{2+} to produce NaCr$_{0.95}$Ni$_{0.05}$O$_2$ as an efficient cathode for these batteries. We found that Ni^{2+} substitution plays a critical role in the ionic character of transition metal-oxygen bonds, which increases the interlayer separation and thus improves sodium-ion diffusion kinetics. Furthermore, Ni^{2+} substitution reduces the deterioration of NaCrO$_2$ throughout charge-discharge processes and thus boosts the cycle performance of the materials. The resultant NaCr$_{0.95}$Ni$_{0.05}$O$_2$ cathode displays a remarkable rate performance with specific capacities of 91.2 mAh g^{-1} at 50 C and a high retention (~80%) of the initial capacity after cycling for 1,000 cycles at 10 C.

Keywords: Sodium-ion battery, electronic structure, charge compensation, rate performance

INTRODUCTION

The emergence of sodium-ion batteries (SIBs) requires efficient and stable cathodes[1,2]. Amongst the most investigated cathodic materials, layered transition metal (TM) oxides have attracted significant attention because of their low-cost synthesis and high theoretical specific capacity[3-6]. For example, $NaCrO_2$ (coded as NCO) has been intensively studied assignable to its flat discharge curves and strong temperature adaptability[7,8]. It is also a well-established cathode material with a capacity of ~120 mAh g^{-1}[9,10]. Nevertheless, the material suffers from a rapid capacity decay at high rate during recycling due to a low Na^+ diffusivity. Additionally, its crystal structure can be damaged during the repeated (de)intercalation of sodium ions, which leads to an irreversible strain accumulation and the fading of the capacity[11].

Different methods such as carbon encapsulation[10,12], morphology control[13,14] and cation substitution[15] have been reported to demolish these obstacles for NCO. Among them, cation substitution has been considered one of the most effective and facile ways to enhance cycling stability and rate capability[16-18]. Cationic substitution refers primarily to replacing parts of TM ions with others. For instance, a delayed phase transition of O3-P3 was observed in the Ti-substituted NCO which achieved a specific discharge capacity of 96.7 mAh g^{-1} at a discharge rate of 1 C and a high capacity retention (~80% after 800 cycles)[19]. Furthermore, Lee *et al.* proposed a co-substitution strategy to reinforce the structural stability of the NCO, allowing the cathode to deliver a high-rate performance (> 20 C) and a long cycle life (> 1,000 cycles)[20]. Following this line, it was found that a substitution of Cr with Sb in NCO could expand the Na^+ transmission channels[21]. Despite these notable advancements, the impact of low-valent TM substitution on electronic structure of layered oxides for SIBs and its subsequent effect on performance improvement have yet to be thoroughly investigated.

Here, we show an effective method to improve comprehensive performance of NCO by Ni^{2+} substitution. The substitution of Cr^{3+} by low-valent Ni^{2+} to produce $NaCr_{0.95}Ni_{0.05}O_2$ influences the ionic character of the TM-oxygen bonds, which, in turn, increases the interlayer spacing of sodium layers to improve the diffusion kinetics of sodium ions. In addition, Ni^{2+} substitution inhibits the structural degradation of NCO during charge-discharge cycling, which effectively enhances the cycling performance of the material. Consequently, the $NaCr_{0.95}Ni_{0.05}O_2$ exhibits an impressive performance of a remarkable rate performance with 91.2 mAh g^{-1} at 50 C and a high retention (80%) of the initial capacity after cycling for 1,000 cycles at 10 C.

RESULTS AND DISCUSSION

The control sample NCO and its derivative $NaCr_{1-x}Ni_xO_2$ with different Ni contents (x = 0.03, 0.05, 0.07, noted as NCNO-x, respectively, in which x represents the moles of Ni^{2+} substitution to Cr^{3+}) were synthesized *via* the solid-phase method[22]. The X-ray diffraction (XRD) patterns in Figure 1A and Supplementary Figure 1 confirm the rhombohedral layered phase for NCO, NCNO-0.03, and NCNO-0.05[14]. An impure phase NiO (marked with asterisk) appears in the NCNO-0.07, which is due to excessive doping of Ni^{2+}[23]. The XRD peaks at 16.65° and 41.70° can be ascribed to the (003) and (104) crystal faces of $Rinem\bar{3}m$ structure, respectively. Figure 1A also presents the magnified XRD patterns correlated to the (003) and (104) planes for the control samples before and after ionic substitution. We noticed that the XRD peaks corresponding to the (003) and (104) planes shift to lower angles as the Ni^{2+} concentration increases, indicating an enlargement of spacing of the corresponding slabs. For XRD characterization, these diffraction peaks at lower 2θ angles indicate larger interplanar spacings, and vice versa[24]. In view of the fact that Na^+ mostly moves across the (003) planes adjacent to the sodium layers, a larger spacing among the (003) slabs could facilitate the diffusion of cations[25]. To gain crystallographic information, we further used Rietveld analysis to refine the XRD patterns of the NCO and NCNO-0.05. Supplementary Figure 2 gives the results. Supplementary Table 1 summarizes the corresponding crystallographic parameters for the NCO and
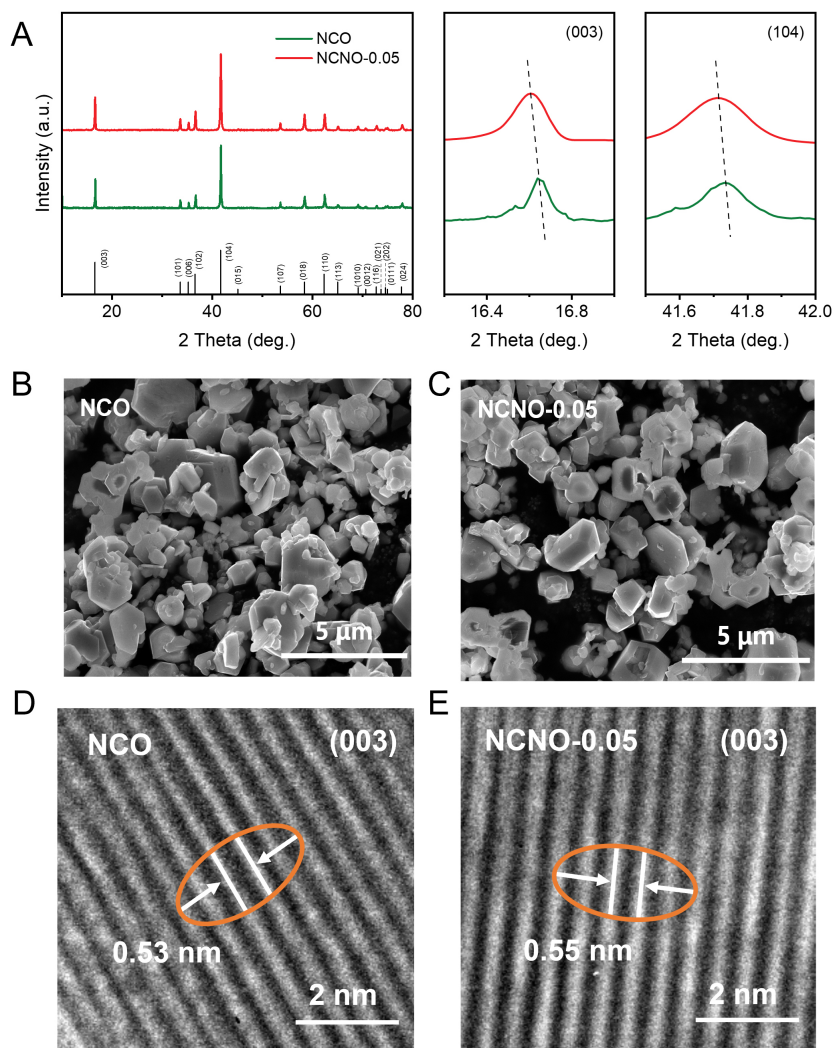
Figure 1. XRD patterns of (A) synthesized samples and the magnified diffraction peaks for the (003) and the (104) planes. SEM images of (B) the NCO and (C) the NCNO-0.05 samples. HRTEM images of (D) the NCO and (E) NCNO-0.05 samples.

the NCNO-0.05 samples. Here, an increase in the lattice parameter a from 2.9697 Å for the NCO to 2.9737 Å for the NCNO-0.05 was observed. Such an increase in the lattice parameter a for the NCNO-0.05 could be ascribed to the comparatively bigger ionic radius of Ni^{2+} (0.69 Å) compared to Cr^{3+} (0.615 Å). A higher lattice parameter a corresponds to an expansion of TM ionic radii on the a-axis, whereas a higher lattice parameter c reflects the effect of the Coulomb repulsion[26]. Likewise, a strong O-O repulsion between nearby TMO_6 layers is responsible for the rise of lattice parameter c from 15.9746 to 15.9966 Å[23]. The high accuracy of the Rietveld refinement results is reflected by the low reliability factors for the NCO (R_p: 6.64%, R_{wp}: 9.11%) and the NCNO-0.05 (R_p: 6.77%, R_{wp}: 8.46%) samples, where R_p is R-pattern and R_{wp} is R-weighted pattern.

Figure 1B and C presents scanning electron microscopy (SEM) images of the corresponding samples featuring micro-particles with an inconsistent configuration. We used the Nano Measurer software to statistically analyze the size distribution of particles. Particle size distribution analysis [Supplementary Figure 3] indicates that the NCNO-0.05 sample ($d_{50} \sim 0.40$ μm) is averagely smaller than the

NCO sample ($d_{50} \sim 0.57$ μm). The energy dispersive spectroscopy mapping image characterization further verifies uniformly dispersed elements in NCNO-0.05 [Supplementary Figure 4], from which the ratio of Cr:Ni was evaluated to be 0.952:0.047 [Supplementary Table 2]. This is further confirmed with the inductively coupled plasma spectroscopy measurement (ratio = 0.946:0.048, Supplementary Table 3).

Figure 1D and E presents the high-resolution transmission electron microscopy (HRTEM) characterization on the NCO and NCNO-0.05 samples, respectively. The original images have been included in Supplementary Figure 5. After Ni^{2+}-substitution, the fringe spacing corresponding to the (003) plane increases from 0.53 to 0.55 nm for the NCNO-0.05 sample, which belongs to the Rinm phase of O3-type layered metal oxide. The wider interlayer distance is beneficial to the faster kinetic[19,27]. Therefore, introduction of Ni^{2+} leads to local adjustment and optimization of the lattice structure, making the lattice more favorable for the accommodation and diffusion of sodium ions.

We further carried out electronic localization function (ELF) calculations to rationalize the influence of Ni substitution onto the electronic structures of samples. Figure 2A illustrates the ELF map of valence electrons at the slices along the (001) plane for the NCO and NCNO-0.05 samples. The value in the two-dimensional ELF slice along (001) surface is in the range between 0 and 1. The value of 1 in red region indicates a complete localization, while that of 0.5 in green region corresponds to a delocalized electron gas. In short, a big ELF value indicates a strong localization of electrons. Therefore, in the ELF profile, compared with those in the NCO sample, the NCNO-0.05 sample shows an easily distinguished electron localization in the O-Cr coordination. This result indicates this bond has a more ionic character within the NCNO-0.05 sample than within NCO[28]. This could be ascribed to the fact that the Cr^{3+} ion has a higher coordination capacity than the Ni^{2+} due to the existence of empty 3d orbitals. In addition, enrichment of electrons between Cr-O could reduce the electrostatic interaction between the electrons and the sodium ions in the interlayer, which favors the diffusion of Na^+[29,30]. This deduction can be explored by the accumulation of electrons on the O atoms to enhance the repulsion between O-O bonds. Previous reports have indicated that an enhancement of the ionic character of the TM-O bond can destabilize the P3 phase by sharing faces between NaO_6 and TMO_6 polyhedra in the layered crystal, thus promoting a reversible transition from the O3 to P3 phase[31,32].

We further carried out X-ray photoelectron spectroscopy (XPS) measurements to examine the chemical states of interested elements in samples. Figure 2B presents the Cr $2p_{3/2}$ XPS signal in which the peaks at binding energies of about 575.1 and 576.2 eV can be ascribed to the Cr^{2+} and Cr^{3+} species[33]. Compared to the NCO sample, the content of Cr^{2+} in the NCNO sample increases from 15.8% to 18.4% for the NCNO-0.05 by integrating the corresponding XPS peaks. Figure 2C illustrates Ni 2p XPS spectra of the NCNO-0.05 electrode, from which the Ni $2p_{3/2}$ peaks at binding energies of about 855.2 eV can be deconvoluted to the Ni^{2+}[34,35]. This result indicates a constant valence of Ni^{2+} after synthesis. This further informs that the change in valence from Cr^{3+} to Cr^{2+} is not caused by electron transfer from the Ni^{2+}. The O 1s spectrum can be divided into three peaks according to different oxygen species [Supplementary Figure 6]: lattice oxygen (O^{2-}) at 528.9 eV, oxygen vacancies (O_V) at 530.6 eV, and surface adsorbed oxygen (surface OH^-/O_2) at 531.8 eV[36,37]. Though it is difficult to evaluate a precise concentration for these species, a relative comparison of weight ratio can give a hint on the change of O_V in samples. By calculating the percentage of each species to the total O 1s XPS, we noticed the ratio of O_V to O^{2-} in the NCNO-0.05 (1.7) is higher than that of NCO samples (1.3), suggesting a higher contribution from O_V upon Ni^{2+} substitution. Moreover, the ratios of O_V to O^{2-} in NCNO-0.03 and NCNO-0.07 are approximately 1.4 and 0.9, respectively. The Ni-substitution-induced augment of O_V concentration in samples could be attributed to two mechanisms. The first involves the reduction of Cr^{3+} cations, where two Cr^{3+} ions are converted into two Cr^{2+} ions, resulting in the creation of one O_V. Alternatively, O_V can be introduced by
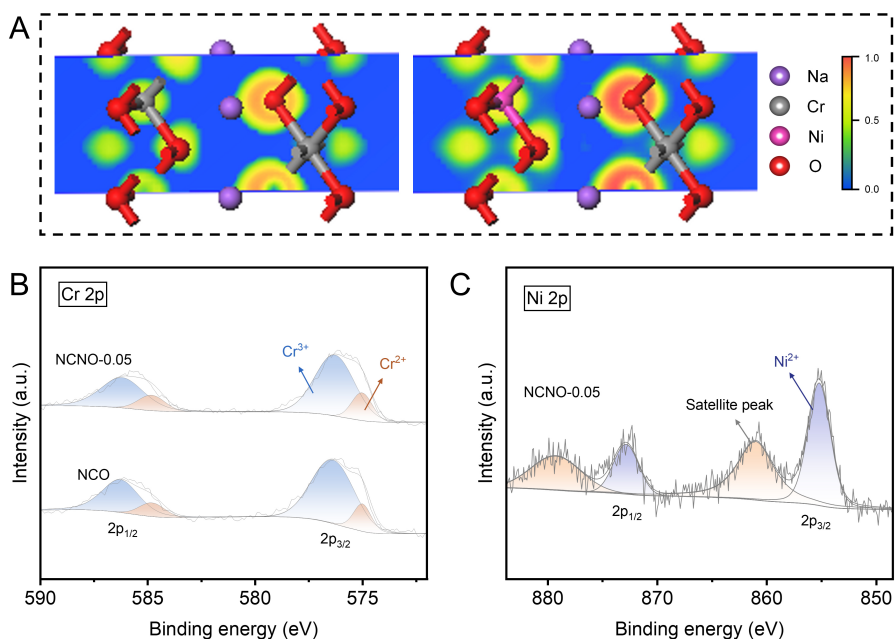
Figure 2. (A) The electron localization function of valence electrons at the slices along the (001) plane of NCO and NCNO-0.05 samples. (B) The Cr 2p XPS spectra of the as-obtained NCO and NCNO-0.05 samples. (C) Ni 2p XPS spectra of NCNO-0.05.

substituting Ni^{2+} cations for Cr^{3+} cations in the lattice[38-42]. Supplementary Figure 7 shows *ex-situ* XPS of Cr 2p and Ni 2p in NCNO-0.05, revealing that only Cr^{3+} is involved in charge compensation when charged to 3.6 V. We also attempted to charge the batteries to 3.8 V. Supplementary Figure 8 exhibits the charge-discharge curves and the capacity differential curves of the NCO and NCNO-0.05 samples. Charging the batteries to 3.8 V enables the Ni^{2+}/Ni^{3+} redox couple to become active and participate in the redox reaction, but unfortunately, it also compromises the structural stability of the material. Consequently, subsequent electrochemical testing was conducted within the voltage range of 2.0-3.6 V.

Several coin-type cells (CR2032) were assembled with the $NaCr_xNi_{1-x}O_2$ samples of various Ni-contents in order to study their performance in a voltage range from 2.0 to 3.6 V (*vs.* Na^+/Na). Figure 3A and Supplementary Figure 9 compare the first curves of charging and discharging processes at 0.2 C for the NCO, NCNO-0.03, NCNO-0.05, and NCNO-0.07 samples. We noticed that the initial discharge capacity increases as the Ni^{2+} content in the samples rises up to 5%. Considering that the NCNO-0.05 sample has the best performance in terms of specific capacity, we then chose this composition for further detailed investigations. The NCNO-0.05 sample achieved a discharge capacity of 120.3 mAh g^{-1} at a rate of 0.2 C, which is higher than the NCO electrode (116.0 mAh g^{-1}). The coulombic efficiency (CE) of the first charge-discharge procedure for the NCNO-0.05 electrode (97.7%) is also higher than that of the NCO electrode (95.6%). The enhancement in initial charge-discharge capacity of NCNO-0.05 is closely associated with the reversible insertion and extraction of sodium ions, as evidenced by the higher Coulombic efficiency. The air stability of NCO and NCNO-0.05 was compared by exposing them to air for 12 h. As shown in the Supplementary Figure 10, NCO displayed a capacity degradation of 2.9 mAh g^{-1}, while NCNO-0.05 showed a slightly higher degradation of 3.3 mAh g^{-1} due to its larger interlayer spacing that facilitates H_2O molecule insertion[43].
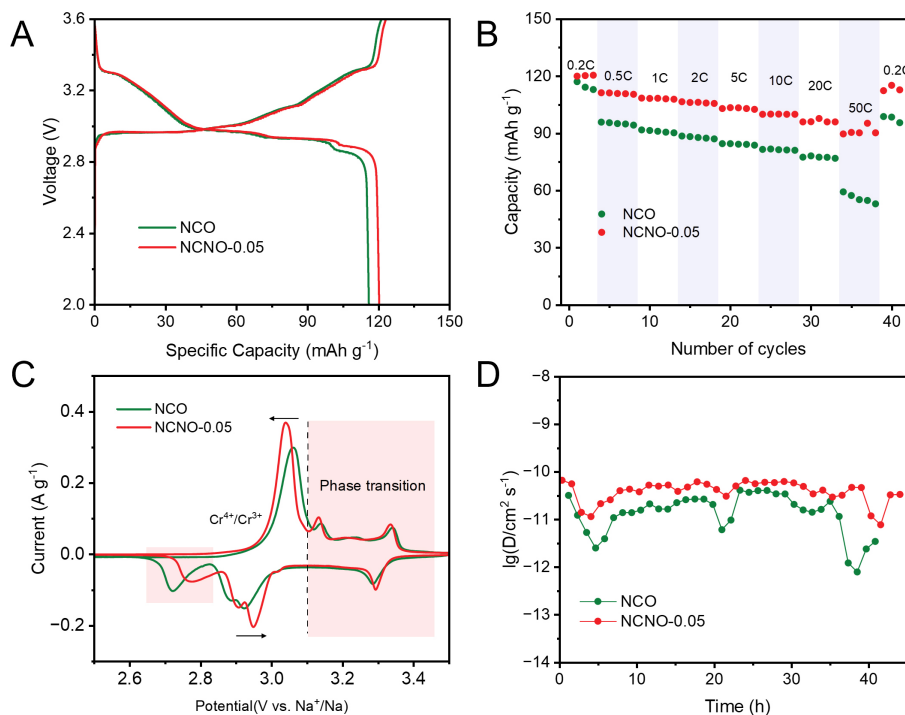
Figure 3. (A) The charge/discharge profiles of CR2032 type coin cells assembled with the prepared the NCO and NCNO-0.05 samples as the working electrode and Na metal as the counter electrode. The charge/discharge rate is 0.2 C. (B) The rate behaviors of CR2032 type coin cells. (C) The cyclic voltammogram curves of the NCO and the NCNO-0.05 electrodes at the first cycle at a scan rate of 0.1 mV^{-1}. (D) The diffusion coefficient of Na$^+$.

Figure 3B compares the rate behavior of the NCO and NCNO-0.05 electrodes. At a discharge rate of 50 C, the NCNO-0.05 electrode retained a capacity of 91.2 mAh g^{-1}, while the NCO electrode presented a much lower capacity (45.3 mAh g^{-1}). After the discharge rate was set back to 0.2 C, the capacities of the NCNO-0.05 and the NCO electrodes were retained to 112.4 and 98.8 mAh g^{-1}, corresponding to 94% and 84% retention of their original capacity, respectively.

Figure 3C shows the cyclic voltammetry (CV) curves for the first charging cycle at a sweep rate of 0.1 mV s^{-1}. The two major redox peaks at 3.04/2.95 V correspond to the redox reaction between Cr^{3+}/Cr^{4+}[13]. The other smaller peaks are likely related to phase transitions in the layered metal oxide structure, as suggested by previous studies[36,44,45]. The NCO cathode material principally operates with the compensation mechanism in terms of deintercalation of Na$^+$ during the charging process and its re-intercalation during the discharging process[46-49]. In the whole procedure, the charge equivalence is sustained by the redox reaction of Cr ions. The separation of the redox peaks of the NCNO-0.05 sample (ΔE = 87 mV) is smaller than that of the NCO sample (ΔE = 145 mV), suggesting that Ni substitution enhances the kinetics dynamics[20]. The diffusion coefficient of Na$^+$ (D_{Na^+}) was further explored with Galvanostatic Intermittent Titration Technique (GITT) characterization[50]. The electrodes were charged at a current density of 20 mA g^{-1} for 15 min, followed by relaxation at open circuit conditions for 1 h [Supplementary Figure 11].

Figure 3D presents the calculated D_{Na^+} from the GITT characterization of both samples. Accordingly, the NCNO-0.05 sample (4.25 × 10^{-11} cm^2 s^{-1}) has a higher calculated average value of D_{Na^+} than the NCO sample (1.84 × 10^{-11} cm^2 s^{-1}), indicating the faster kinetic of Na$^+$ diffusion in the NCNO-0.05 sample. As a result, sodium storage can be facilitated by the facile transfer of sodium ions, leading to an excellent rate performance[51].

Figure 4A shows the cycling stability for the prepared samples. The discharge capacities of the NCO and NCNO-0.05 electrodes at a rate of 10 C after 500 cycles were retained to 50.4 and 89.4 mAh g^{-1}, with the capacity retentions of 52% and 88%, respectively. After 1,000 cycles at a rate of 10 C, the NCNO-0.05 sample showed a discharge capacity of 81 mAh g^{-1}, higher than the NCO electrode of a corresponding capacity of 39.1 mAh g^{-1}. The capacity retention was 80% for the NCNO-0.05 and 40% for the NCO electrode. The capacity loss ratio at a rate of 10 C corresponding to each cycle was 0.060% and 0.021% for the NCO and NCNO-0.05 electrodes, respectively. The rate capability and cycle performance of $NaCr_{0.95}Ni_{0.05}O_2$ are higher than those of $Na_{0.88}Cr_{0.88}Ru_{0.12}O_2$ (83.6 mAh g^{-1} at 50 C) and $Na_{0.9}Ca_{0.05}CrO_2$ (50 mAh g^{-1} at 20 C) (see Supplementary Table 4). Supplementary Table 4 compares the electrochemical properties of NCO-based cathodes.

We further reduced the current density to 5 C in order to observe in more detail the performance of the electrode materials [Figure 4B and C]. The cycling performance comparison underscores the superiority of the NCNO-0.05 electrode, which maintains the capacity retention of 91.6% after 100 cycles at 5 C [Figure 4C], far surpassing the 75.4% retention demonstrated by the NCO electrode [Figure 4B]. In addition, the NCO electrode experienced severe voltage decay during cycling as indicated by the slanted arrows in Figure 4B, which could be related to the structural degradation of the material. In contrast, the capacity of NCNO-0.05 is well preserved after cycles.

To verify the structural stability of the NCO and NCNO-0.05 electrodes after different cycles (with a state of charge, SOC = 0%), we further characterized them using XRD. Figure 4D and E presents the results of XRD characterization of the (003) phase. The whole XRD pattern is shown in Supplementary Figure 12. Along with a decrease in diffraction peak intensity, the XRD signal peak for the NCO sample at the (003) phase showed a distinct shift to a lower angle after 100 cycles of sodium-ion intercalation/deintercalation. It suggests that the layered structure has introduced more stacking faults due to repeated volume changes of lattice[47,51]. On the contrary, the XRD signal for the (003) phases of the NCNO-0.05 electrode is well preserved even after 100 cycles. This result verifies the improved stabilization of the O3 structure by Ni^{2+} substitution, which correlates to a highly reversible sodium-ion intercalation/deintercalation for this sample. In short, the highly stable material structure and reversible electrochemical reaction guarantee a long cycle life of Ni^{2+}-substituted NCO.

CONCLUSIONS

In summary, we propose $NaCr_{0.95}Ni_{0.05}O_2$ as a promising cathode for high-efficiency SIBs. The chemical substitution of Cr^{3+} by low-valent Ni^{2+} in NCO can be an attractive method to simultaneously expand the sodium-ion diffusion channel and stabilize the structure during Na$^+$ (de)intercalation. The $NaCr_{0.95}Ni_{0.05}O_2$ has achieved a high capacity (120.3 mA h g^{-1} at 0.2 C), rate performance (91.2 mA h g^{-1} at 50 C), and outstanding long cyclic life (80% after 1,000 cycles at 10 C). Moreover, our research suggests that Ni^{2+} substitution strategies can be extended to other Na-layered oxides. By optimizing the ionic of the TM-O bonds, the properties of layered oxide cathodes can be tailored for improved electrochemical performance.

EXPERIMENTAL

A solid phase reaction was used to synthesize $NaCr_{1-x}Ni_xO_2$ (x = 0, 0.03, 0.05, 0.07). A slight excess of 5 mol% Na_2CO_3 was used to compensate for the loss of sodium volatility. A mixture of Na_2CO_3 (99.8%, Shanghai Macklin Biochemical Co., Ltd.), Cr_2O_3 (99%, Sinopharm Chemical Reagent CO., Ltd.), and NiO (99%, Shanghai Aladdin Biochemical Technology CO., Ltd.) was prepared in a stoichiometric ratio and
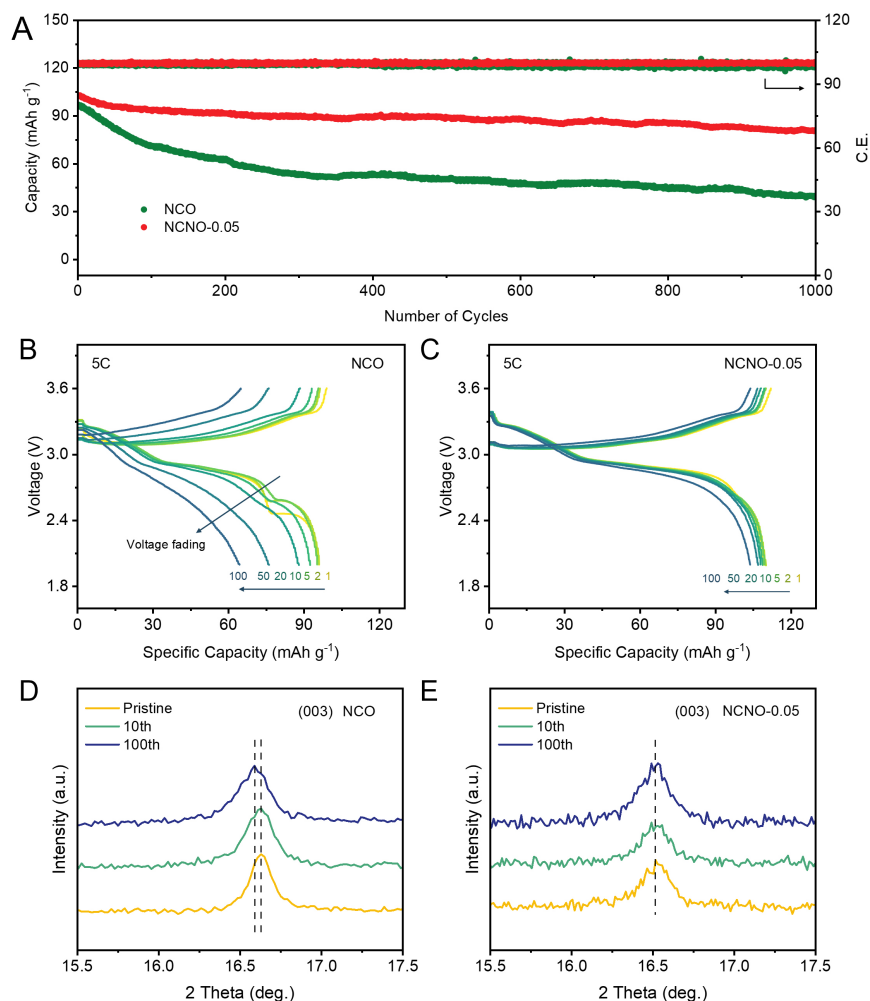
Figure 4. (A) The cycling performances of CR2032 type coin cells at a rate of 10 C. Charge-discharge profiles of (B) NCO and (C) NCNO-0.05 at 5 C. XRD patterns for the (003) of the (D) NCO and (E) NCNO after 0, 10th, and 100th cycles.

thoroughly mixed by ball-milling with ethanol as a dispersing agent for 10 h. The powder was then heated to 900 °C for 5 h in an alumina crucible in an argon atmosphere at a rate of 5 °C per min with a gas flow rate of 100 mL min^{-1}. After cooling to room temperature, the samples were immediately put into a vacuum glove box.

The details about material characterization and electrochemical characterization of the samples are given in the supporting information.

DECLARATIONS
Authors' contributions
Investigation, writing-original draft: Cai J
Investigation: Zhu Y, Zhang J, Tian L, Gao P, Zhang Y
DFT calculation: Zhang Z
Supervision, writing - review & editing: Shen Y
Writing - review & editing: Wang M

Conflicts of interest

All authors declared that there are no conflicts of interest.

Ethical approval and consent to participate

Not applicable.

Consent for publication

Not applicable.

Copyright

REFERENCES

1. Huang Y, Zheng Y, Li X, et al. Electrode materials of sodium-ion batteries toward practical application. *ACS Energy Lett* 2018;3:1604-12. DOI
2. Eng AYS, Soni CB, Lum Y, et al. Theory-guided experimental design in battery materials research. *Sci Adv* 2022;8:eabm2422. DOI PubMed PMC
3. Du M, Du K, Guo J, et al. Direct reuse of oxide scrap from retired lithium-ion batteries: advanced cathode materials for sodium-ion batteries. *Rare Met* 2023;42:1603-13. DOI
4. Huang Z, Zhang X, Zhao X, et al. Hollow $Na_{0.62}K_{0.05}Mn_{0.7}Ni_{0.2}Co_{0.1}O_2$ polyhedra with exposed stable {001} facets and K riveting for sodium-ion batteries. *Sci China Mater* 2023;66:79-87. DOI
5. Huang Z, Zhang X, Zhao X, et al. Suppressing oxygen redox in layered oxide cathode of sodium-ion batteries with ribbon superstructure and solid-solution behavior. *J Mater Sci Technol* 2023;160:9-17. DOI
6. Komaba S, Murata W, Ishikawa T, et al. Electrochemical Na insertion and solid electrolyte interphase for hard-carbon electrodes and application to Na-ion batteries. *Adv Funct Mater* 2011;21:3859-67. DOI
7. Kubota K, Ikeuchi I, Nakayama T, et al. New insight into structural evolution in layered $NaCrO_2$ during electrochemical sodium extraction. *J Phys Chem C* 2015;119:166-75. DOI
8. Xia X, Dahn JR. $NaCrO_2$ is a fundamentally safe positive electrode material for sodium-ion batteries with liquid electrolytes. *Electrochem Solid State Lett* 2012;15:A1. DOI
9. Yu C, Park J, Jung H, et al. $NaCrO_2$ cathode for high-rate sodium-ion batteries. *Energy Environ Sci* 2015;8:2019-26. DOI
10. Ikhe AB, Park WB, Manasi M, Ahn D, Sohn KS, Pyo M. Unprecedented cyclability and moisture durability of $NaCrO_2$ sodium-ion battery cathode via simultaneous Al doping and Cr_2O_3 coating. *ACS Appl Mater Interfaces* 2023;15:14958-69. DOI
11. Wable M, Bal B, Capraz ÖÖ. Probing electrochemical strain generation in sodium chromium oxide ($NaCrO_2$) cathode in Na-ion batteries during charge/discharge. *Energy Adv* 2024;3:601-8. DOI
12. Ding J, Zhou Y, Sun Q, Fu Z. Cycle performance improvement of $NaCrO_2$ cathode by carbon coating for sodium ion batteries. *Electrochem Commun* 2012;22:85-8. DOI
13. Liang L, Zhang W, Denis DK, et al. Comparative investigations of high-rate $NaCrO_2$ cathodes towards wide-temperature-tolerant pouch-type Na-ion batteries from -15 to 55 °C: nanowires *vs.* bulk. *J Mater Chem A* 2019;7:11915-27. DOI
14. Liang L, Sun X, Denis DK, et al. Ultralong layered $NaCrO_2$ nanowires: a competitive wide-temperature-operating cathode for extraordinary high-rate sodium-ion batteries. *ACS Appl Mater Interfaces* 2019;11:4037-46. DOI

15. Wang Y, Cui P, Zhu W, et al. Enhancing the electrochemical performance of an O_3-$NaCrO_2$ cathode in sodium-ion batteries by cation substitution. *J Power Sources* 2019;435:226760. DOI

16. Li Y, Chen M, Liu B, Zhang Y, Liang X, Xia X. Heteroatom doping: an effective way to boost sodium ion storage. *Adv Energy Mater* 2020;10:2000927. DOI

17. Li XL, Bao J, Li YF, et al. Boosting reversibility of Mn-based tunnel-structured cathode materials for sodium-ion batteries by magnesium substitution. *Adv Sci* 2021;8:2004448. DOI PubMed PMC

18. Xi K, Chu S, Zhang X, et al. A high-performance layered Cr-based cathode for sodium-ion batteries. *Nano Energy* 2020;67:104215. DOI

19. Li W, Wang Y, Hu G, et al. Ti-doped $NaCrO_2$ as cathode materials for sodium-ion batteries with excellent long cycle life. *J Alloys Compd* 2019;779:147-55. DOI

20. Lee I, Oh G, Lee S, et al. Cationic and transition metal co-substitution strategy of O_3-type $NaCrO_2$ cathode for high-energy sodium-ion batteries. *Energy Stor Mater* 2021;41:183-95. DOI

21. Xu H, Yan Q, Yao W, Lee C, Tang Y. Mainstream optimization strategies for cathode materials of sodium-ion batteries. *Small Struct* 2022;3:2100217. DOI

22. Ko W, Cho M, Kang J, et al. Exceptionally increased reversible capacity of O_3-type $NaCrO_2$ cathode by preventing irreversible phase transition. *Energy Stor Mater* 2022;46:289-99. DOI

23. Ma C, Li X, Yue X, Bao J, Luo R, Zhou Y. Suppressing O3-O'3 phase transition in $NaCrO_2$ cathode enabling high rate capability for sodium-ion batteries by Sb substitution. *Chem Eng J* 2022;432:134305. DOI

24. Wang Y, Yang Z, Qian Y, Gu L, Zhou H. New insights into improving rate performance of lithium-rich cathode material. *Adv Mater* 2015;27:3915-20. DOI

25. Liu Y, Jiang W, Ling M, Fan X, Wang L, Liang C. Revealing lithium configuration in aged layered oxides for effective regeneration. *ACS Appl Mater Interfaces* 2023;15:9465-74. DOI

26. Biasi L, Kondrakov AO, Geßwein H, Brezesinski T, Hartmann P, Janek J. Between scylla and charybdis: balancing among structural stability and energy density of layered NCM cathode materials for advanced lithium-ion batteries. *J Phys Chem C* 2017;121:26163-71. DOI

27. Zhao C, Yao Z, Wang Q, et al. Revealing high Na-content P2-type layered oxides as advanced sodium-ion cathodes. *J Am Chem Soc* 2020;142:5742-50. DOI

28. Zhai Y, Yang W, Ning D, et al. Improving the cycling and air-storage stability of $LiNi_{0.8}Co_{0.1}Mn_{0.1}O_2$ through integrated surface/interface/doping engineering. *J Mater Chem A* 2020;8:5234-45. DOI

29. Feng J, Luo SH, Qian L, et al. Properties of the "Z"-phase in Mn-rich P2-$Na_{0.67}Ni_{0.1}Mn_{0.8}Fe_{0.1}O_2$ as sodium-ion-battery cathodes. *Small* 2023;19:e2208005. DOI

30. Wang H, Gao X, Zhang S, et al. High-entropy Na-deficient layered oxides for sodium-ion batteries. *ACS Nano* 2023;17:12530-43. DOI

31. Wang PF, Xin H, Zuo TT, et al. An abnormal 3.7 volt O3-type sodium-ion battery cathode. *Angew Chem Int Ed* 2018;57:8178-83. DOI

32. Sathiya M, Jacquet Q, Doublet M, Karakulina OM, Hadermann J, Tarascon J. A chemical approach to raise cell voltage and suppress phase transition in O3 sodium layered oxide electrodes. *Adv Energy Mater* 2018;8:1702599. DOI

33. Chu S, Kim D, Choi G, et al. Revealing the origin of transition-metal migration in layered sodium-ion battery cathodes: random Na extraction and Na-free layer formation. *Angew Chem Int Ed* 2023;62:e202216174. DOI

34. Wang PF, You Y, Yin YX, et al. Suppressing the P2-O2 phase transition of $Na_{0.67}Mn_{0.67}Ni_{0.33}O_2$ by magnesium substitution for improved sodium-ion batteries. *Angew Chem Int Ed* 2016;55:7445-9. DOI

35. Zhou Y, Ding J, Nam K, et al. Phase transition behavior of $NaCrO_2$ during sodium extraction studied by synchrotron-based X-ray diffraction and absorption spectroscopy. *J Mater Chem A* 2013;1:11130. DOI

36. Ma Q, Chen Z, Zhong S, et al. Na-substitution induced oxygen vacancy achieving high transition metal capacity in commercial Li-rich cathode. *Nano Energy* 2021;81:105622. DOI

37. Guo W, Zhang C, Zhang Y, et al. A universal strategy toward the precise regulation of initial coulombic efficiency of Li-rich Mn-based cathode materials. *Adv Mater* 2021;33:e2103173. DOI

38. Lin C, Meng X, Liang M, et al. Facilitating reversible transition metal migration and expediting ion diffusivity *via* oxygen vacancies for high performance O3-type sodium layered oxide cathodes. *J Mater Chem A* 2022;11:68-76. DOI

39. Wang W, He R, Wang Y, et al. Boosting methanol-mediated CO_2 hydrogenation into aromatics by synergistically tailoring oxygen vacancy and acid site properties of multifunctional catalyst. *Chemistry* 2023;29:e202301135. DOI

40. Cui SL, Zhang X, Wu XW, et al. Understanding the structure-performance relationship of lithium-rich cathode materials from an oxygen-vacancy perspective. *ACS Appl Mater Interfaces* 2020;12:47655-66. DOI

41. Carey JJ, Legesse M, Nolan M. Low valence cation doping of bulk Cr_2O_3: charge compensation and oxygen vacancy formation. *J Phys Chem C* 2016;120:19160-74. DOI

42. Moltved KA, Kepp KP. The chemical bond between transition metals and oxygen: electronegativity, d-orbital effects, and oxophilicity as descriptors of metal-oxygen interactions. *J Phys Chem C* 2019;123:18432-44. DOI

43. Li H, Wang J, Xu S, et al. Universal design strategy for air-stable layered Na-ion cathodes toward sustainable energy storage. *Adv Mater* 2024;36:e2403073. DOI

44. Hou P, Gong M, Tian Y, Li F. A new high-valence cation pillar within the Li layer of compositionally optimized Ni-rich $LiNi_{0.9}Co_{0.1}O_2$ with improved structural stability for Li-ion battery. *J Colloid Interface Sci* 2024;653:129-36. DOI

45. Wang Y, Feng Z, Cui P, et al. Pillar-beam structures prevent layered cathode materials from destructive phase transitions. *Nat Commun* 2021;12:13. DOI PubMed PMC

46. Wang S, Chen F, Zhu TY, et al. In situ-formed Cr_2O_3 Coating on $NaCrO_2$ with improved sodium storage performance. *ACS Appl Mater Interfaces* 2020;12:44671-8. DOI

47. Wang Y, Li W, Hu G, et al. Electrochemical performance of large-grained $NaCrO_2$ cathode materials for Na-ion batteries synthesized by decomposition of $Na_2Cr_2O_7 \cdot 2H_2O$. *Chem Mater* 2019;31:5214-23. DOI

48. Konarov A, Choi JU, Bakenov Z, Myung S. Revisit of layered sodium manganese oxides: achievement of high energy by Ni incorporation. *J Mater Chem A* 2018;6:8558-67. DOI

49. Luo K, Roberts MR, Hao R, et al. Charge-compensation in 3*d*-transition-metal-oxide intercalation cathodes through the generation of localized electron holes on oxygen. *Nat Chem* 2016;8:684-91. DOI

50. Ding F, Zhao C, Xiao D, et al. Using high-entropy configuration strategy to design Na-ion layered oxide cathodes with superior electrochemical performance and thermal stability. *J Am Chem Soc* 2022;144:8286-95. DOI

51. Liu T, Liu J, Li L, et al. Origin of structural degradation in Li-rich layered oxide cathode. *Nature* 2022;606:305-12. DOI